

Compositional effects on the interband transition in GaAs_{1-x}P_x ternary alloys

S. S. CETIN^{a*}, T. S. MAMMADOV^{a, b}, S. OZCELIK^a

^aGazi University, Department of Physics, Teknikokullar, Ankara 06500, Turkey

^bNational Academy of Science, Institute of Physics, Baku, Azerbaijan

GaAs_{1-x}P_x/GaAs alloys were grown on Si-GaAs (100) substrate by solid source molecular beam epitaxy (MBE) technique using GaP decomposition source. The critical point (CP) energies of the interband-transition edges of the structures were determined by line-shape analyses on their dielectric functions measured by spectroscopic ellipsometry (SE) at room temperature in the 0.5-5 eV photon energy regions. We obtained a new bowing parameter by analyzing effect of the phosphorous compositions on the E₀ transition energy. The band gap energies of the alloys and their bowing value were also obtained by evaluating photoluminescence (PL) emission peak positions at the room temperature.

(Received July 27, 2009; accepted September 5, 2009)

Keywords: MBE, GaAsP, Spectroscopic ellipsometry, Critical points, Photoluminescence

1. Introduction

GaAs_{1-x}P_x ternary alloys are of great technological interest for optoelectronic applications. In particular, GaAsP alloys with wide band gap offer significant advantages for semiconductor devices such as solar cell, red light emitting diode and long-wavelength surface emitting lasers applications [1-3]. GaAsP and other III-V group ternary semiconductor structures have been grown with several techniques such as MOCVD, MBE, etc [4, 5]. The film and interface quality of the structures strongly depends on the growth conditions, such as growth procedure, the flow rate of the species of the alloy and growth temperature. The GaAs/GaAs_{1-x}P_x strained superlattice structures have also plays an important role in the obtaining polarized electron photoemission as cathode [6, 7]. Recently, several researchers have studied to improve the quality of this type structures using different growth conditions or procedure [8, 9]. The growth methods such as growth interrupt, continuously growth (CG) [10] and graded growth (GG) beside of the growth conditions as substrate temperature and flux of the source materials affect the quality phosphorous based heterostructure [8, 11]. The P/As flux ratio is other important parameter for electrical and optical properties and also interface of the layers of this type structures.

The knowledge about the optical and structural properties of materials using for fabrication of semiconductor devices are important. However, optical studies of the critical point (CP) energies for explanation of the energy band structure of pn-junction GaAsP heterostructures is limited number in the literature [12,13]. Dielectric functions (DF) which include experimental

information on the material interband-transitions can be used to explanation of the energy band structure of the semiconductors [14]. In addition, CP energies analysis of DF [$\epsilon(E)$] obtained from spectroscopic ellipsometer (SE) measurement can be used to determine the compositions of semiconductor alloys [15]. However, alloy compositions and the layer thickness of the heterostructures can be precisely determined by using high resolution X-ray diffraction HRXRD [16].

In the present work, GaAs_{1-x}P_x ternary alloy films with various compositions were grown on GaAs(100) substrates by using MBE with together CG and GG methods in order to obtain smooth interface and lattice mismatch structures. The phosphorous compositions of the alloys were determined by HRXRD measurements. Critical energy points of the interband-transition edges, E₀, E₁, E₁+ Δ_1 , E₀' , and E₂, are determined by line-shape analyses by using the DF data obtained SE measurements and their second-derivative spectra ($d^2\epsilon/dE^2$). The band gap energies of the ternary alloys were also estimated by the photoluminescence (PL) emission peak positions at the room temperature. Also, a new bowing parameter of the band gap energy due to disorder phosphorous content was obtained from SE and PL studies.

2. Experimental procedure

pn-junction GaAs_{1-x}P_x samples with various phosphorous compositions have been grown by solid source V80H-MBE system on (100) n-GaAs epi-ready substrate with CG and GG methods using GaP compound source to produce P₂ beam. A cracker cell was used to

obtain dimer arsenic (As₂) beam. Growth of the sample structures were organized as follow: Oxide desorption was terminated under As₂ flux at 670 C°. The temperatures were measured by thermocouple. (2x4) surface reconstructure was observed from reflection high energy electron diffraction (RHEED) system before starting growth. A 0.5 μm thick n-GaAs buffer layer was grown to trap impurities that may diffuse from the substrate at 650 C°. To obtain the lattice match structure, a 1 μm graded index n-GaAs_{1-x}P_x layer was grown. During the growth of this layer, P₂ flux for the each sample was changed from zero to desired flux value on the buffer layer. After the reached the desired P₂ flux value, a 0.5 μm n-GaAs_{1-x}P_x layer was grown. Finally, p-type GaAsP layer was grown at the same temperature with different thickness. Si and Be were incorporated as an n-type and p-type dopant, respectively. The growth rate was 1 μm/h for all layers and Ga flux were kept as a constant value during the growth of the GaAsP layers. The grown GaAs_{1-x}P_x/GaAs heterostructures were schematically presented in Fig.1. The P/As flux ratio was changed to obtaining different phosphorous compositions in the grown samples. The growth conditions such as V/III flux ratio, P/As flux ratio and growth temperatures were listed in Table 1.

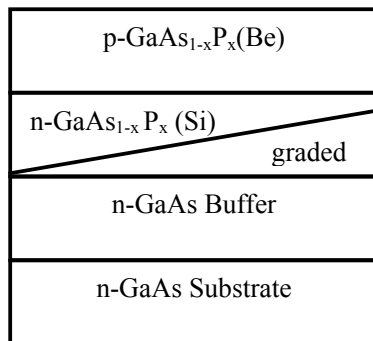


Fig. 1. Schematically representation of the grown GaAs_{1-x}P_x/GaAs heterostructures.

Table 1. V/III flux ratio, P/As flux ratio and growth temperature for GaAsP layers.

Samples	V/III flux ratio (I _{As} + I _P)/I _{Ga}	flux ratio (I _P / I _{As})	Growth temp. (°C)
A1	7	1.5	600
A2	7	2	600
A3	5	2.5	520
A4	5	3.5	520
A5	5	4.6	520

X-ray measurements were carried out on a D-8 Bruker high-resolution diffractometer by using CuKα₁ (1.540Å) radiation, a prodded mirror, and a 4-bounce Ge (220) symmetric monochromator, with the Si calibration sample; its best resolution was 16 arcsec. SE measurements were obtained by using the Jobin Yvon, in 0.5-5 eV photon energy region with an energy resolution of 0.01 eV, at angle of incidence in 70° at the room temperature. Room temperature PL measurements were performed by using the Jobin Yvon Florog-550 PL system with a 50 mW He-Cd laser (λ=325 nm) as an excitation light source.

3. Results and discussion

HRXRD ω-2θ scan of the GaAs_{1-x}P_x structures (A1-A5) are given in Fig.2. In the figure, the high intensity peak comes from GaAs substrate. Other peak corresponds to GaAsP layers. As seen in this figure, the GaAsP peak position is separated from GaAs peak according to phosphorous (P) compositions. The linear region between these two peaks is explained as the existent of graded index layer in the structure. The average phosphorous composition can be calculated from the angular separation of the GaAsP peak with respect to the main GaAs peak. By using the XRD data, the estimated phosphorous content x in alloys A1-A5 have been found as 7%, 15%, 23%, 32% and 39%. The varying of phosphorous content in the samples has been mainly depended on P/As flux ratio as seen in Table 1.

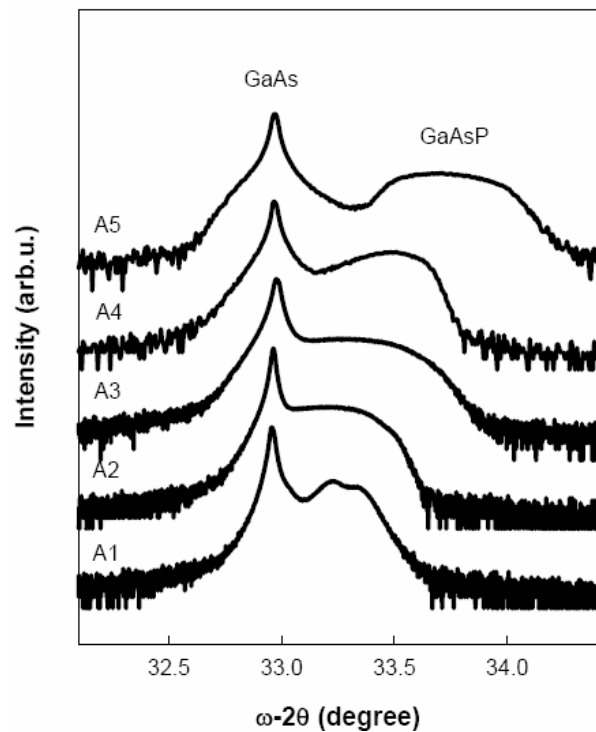


Fig. 2. ω-2θ X-ray diffraction spectrum shows (004) symmetric planes of the epilayers for the structures.

Dielectric functions (DF) which include experimental information on the material interband-transitions can be used to explanation of the energy band structure of the semiconductors. SE measurements were obtained at room temperature with a spectroscopic ellipsometry which is described in Sec.2. The complex reflectance ratio polarized light $R = \frac{r_p}{r_s} = \tan(\Psi) e^{i\Delta}$ determines by this optical technique. Where, r_p and r_s are the reflection coefficient of the polarized light (p and s refers to parallel and perpendicular to the plane of incidence, respectively) and Ψ and Δ are ellipsometric data. The dielectric function $\epsilon = \epsilon_1 + i\epsilon_2$ (ϵ_1 and ϵ_2 are real and imaginary part of the DF, respectively) of the sample was obtained from equation [17]

$$\epsilon = \sin^2\phi + \sin^2\phi \tan^2(\Psi) \frac{(1-\epsilon_1)}{(1+\epsilon_1)} \quad (1)$$

where ϕ is angle of incidence of the light beam.

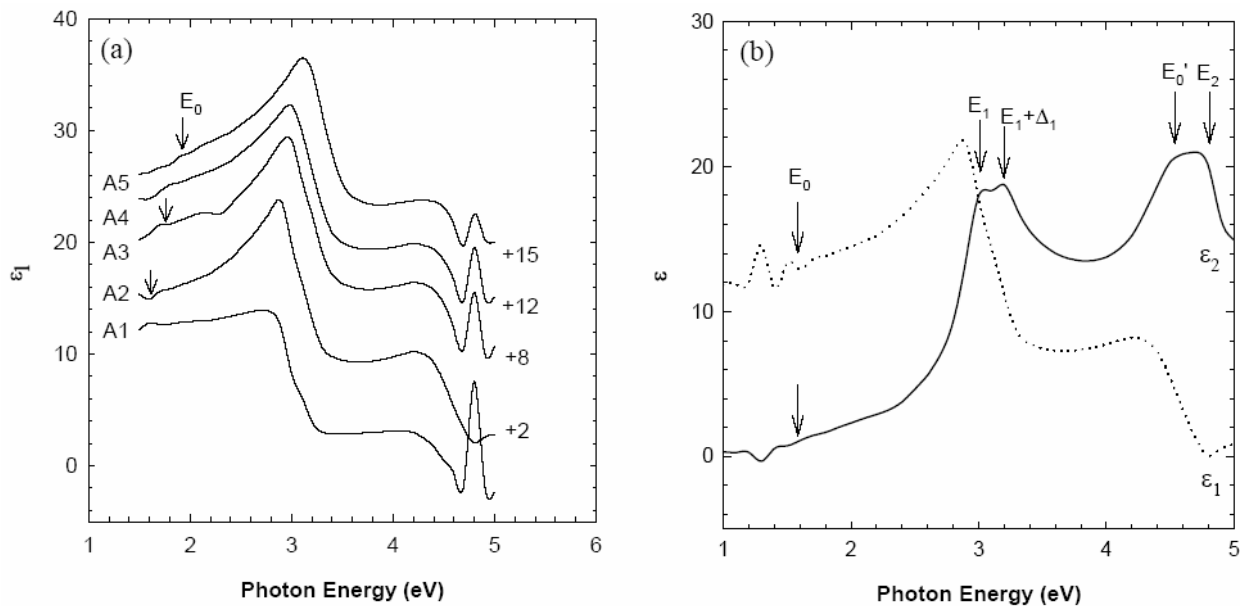


Fig. 3. (a) The real parts of the dielectric functions of GaAs_{1-x}P_x alloys (b) imaginary and real parts of the dielectric function of Sample A2.

These data are not corresponded to accurate CP energies. An analyzing model is necessary in order to obtain accurate energies from ellipsometric data. In literature, there are several models developed for this aim [18-21]. In this work, we used following algorithm to determine the suitable CP energies of the GaAsP ternary alloys from DF spectra. In this model, DF depended on CP energies (E_c) are given by [17]

$$\epsilon(E) = C - A e^{i\phi} (E - E_c + i\Gamma)^{-n} \quad (2)$$

where A is the amplitude, E is the photon energy, E_c is the critical-point energy, Γ is the broadening factor and ϕ is the excitonic phase angle.

SE measurements for all samples were taken at an angle of incidence 70°. The real parts of the dielectric function spectra ϵ_1 of the all samples (A1-A5) were presented in Fig. 3 (a) in the photon energies range of 1.5-5 eV. The dielectric functions (DF) of the sample A2 were shown in Fig. 3(b) as an example. As seen in Fig. 3 (a), E_0 and critical point energies have blue-shifted with increasing phosphorous content in the structures as expected. In the imaginary part of the DF ϵ_2 spectra were observed five peaks as seen in Fig. 3 (b) which correspond to the critical point (CP) energies of the interband-transition edges: E_0 , E_1 , $E_1 + \Delta_1$, E_0' , and E_2 , respectively. These CP energies of sample A2 were estimated at 1.60, 3.00, 3.20, 4.43 and 4.78 eV from ϵ_2 spectra in Fig. 3(b), respectively.

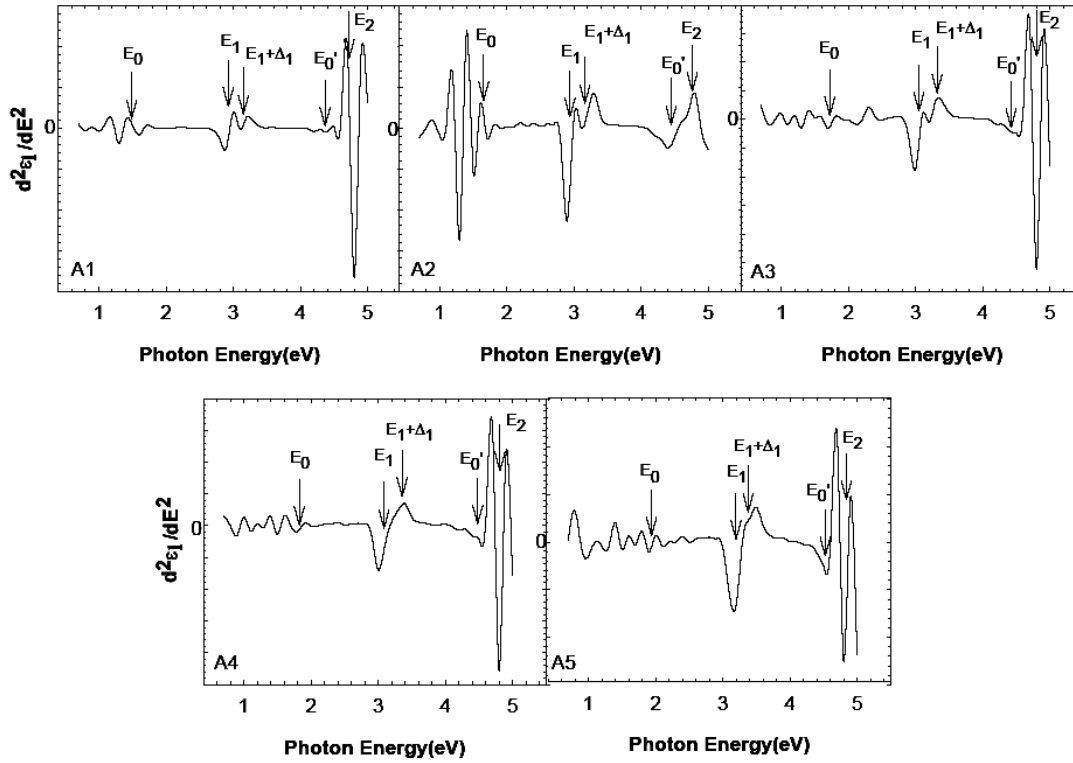


Fig. 4. Second derivative of the real part of dielectric functions spectra of GaAs_{1-x}P_x structures (A1-A5).

We have calculated numerically the second-derivative spectra (in Fig.4), $d^2\varepsilon/dE^2$, of the real parts of experimental DF to perform the line-shape analyses. Calculated second-derivative spectra have been fitted to standard critical-point line shapes represent by

$$\frac{d^2\varepsilon}{dE^2} = -n(n-1)A\varepsilon^{1/2}(E-E_c+\Gamma)^{n-2}, n \neq 0 \quad (3a)$$

$$= A\varepsilon^{1/2}(E-E_c+\Gamma)^{-2}, n = 0, \quad (3b)$$

The exponent n has the values of $-1/2$, 0 , $1/2$, and -1 for the one-dimensional, two-dimensional, three-dimensional, and excitonic critical points, respectively [13]. To determine the E_1 , $E_1+\Delta_1$ and E_0' CPs, the spectra were fitted by the excitonic and the three-dimensional line shape for all samples, respectively. For the E_2 and E_0 CPs,

they were fitted by two-dimensional line shape. Lautenschlager et al. analyzed the structures (Cd_{1-x}Mn_xTe) only in the real part of the dielectric function due to the poor accuracy of the values of ε_2 for small ε_2 in rotating analyzer ellipsometers without compensator [22]. We have also used the second derivative spectrum of ε_1 to estimate peak positions from CP analysis. The CP energies of the interband-transition edges of GaAs_{1-x}P_x alloys have been obtained by using above mentioned method, and they are presented in Fig. 5. Critical point energies, E_0 , E_1 , $E_1+\Delta_1$, E_0' , and E_2 values of GaAs and GaP were taken by Ref.13. Also, the obtained the best-fit critical point parameters E_c and Γ are listed in Table 2 with its errors. The obtained values from the fits are agreement with estimated values from imaginer part of DF for the sample A2 given in Fig. 3 (b).

Table 2. Critical point energies and broadening parameters for GaAs_{1-x}P_x/GaAs structures. Errors are given in parentheses.

Energy (eV)	x=7%	x=15%	x=23%	x=32%	x=39%
E_0	1.510 (0.005)	1.620 (0.002)	1.710 (0.004)	1.780 (0.005)	1.910 (0.004)
E_1	2.938 (0.003)	2.969 (0.001)	3.051 (0.003)	3.061 (0.004)	3.190 (0.006)
$E_1+\Delta_1$	3.177 (0.005)	3.178 (0.003)	3.305 (0.007)	3.350 (0.007)	3.367 (0.027)
E_0'	4.370 (0.001)	4.400 (0.001)	4.440 (0.001)	4.470 (0.004)	4.540 (0.002)
E_2	4.740 (0.007)	4.750 (0.001)	4790 (0.004)	4.790 (0.007)	4.820 (0.013)
Γ_0	0.0377 (0.005)	0.0510 (0.002)	0.0536 (0.003)	0.0611 (0.011)	0.0714 (0.011)
Γ_1	0.1167 (0.003)	0.1252 (0.001)	0.1530 (0.004)	0.1710 (0.003)	0.1860 (0.003)
$\Gamma_1+\Delta_1$	0.1490 (0.004)	0.1579 (0.004)	0.1874 (0.020)	0.1913 (0.010)	0.1991 (0.026)

The phosphorous effect on the CPs for the GaAs_{1-x}P_x structure has been observed. As seen in Fig.5, the E₁, E₁+Δ₁, E'₀, and E₂ edges of the alloys shift linearly to higher energies (blue-shifted) and the spin-orbit splitting (Δ₁) energy decreases as the phosphorous composition increases.

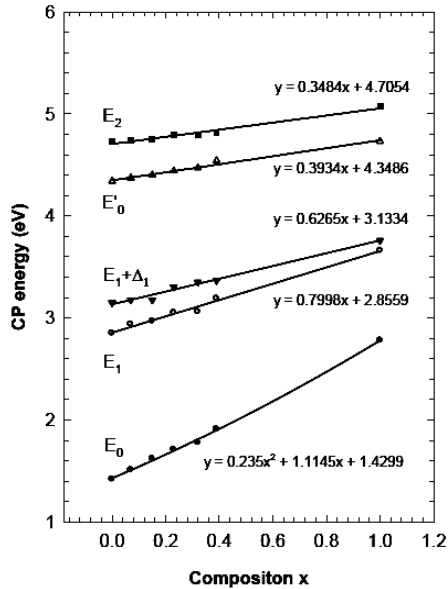


Fig. 5. Evaluation of E₀, E₁, E₁+Δ₁, E'₀, and E₂ transition edges of GaAs_{1-x}P_x with the composition x.

However, the E₀ edge of the structures has shifted to high energies (blue-shifted) with a positive bowing as phosphorous composition increases. Similar behavior was observed in Ref. 13. In our calculations, the bowing parameter (b) has been obtained as 0.235 eV.

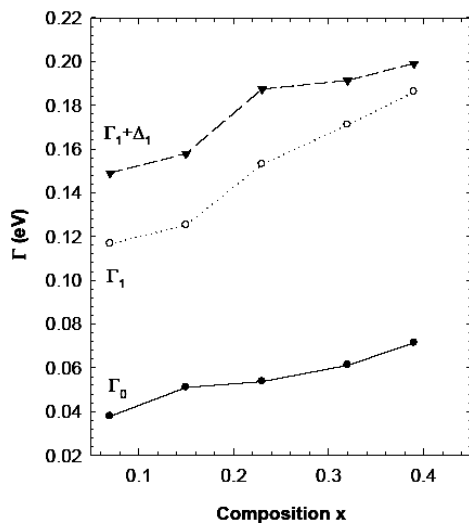


Fig. 6. Broadening parameters (Γ_0 , Γ_1 , and $\Gamma_1+\Delta_1$) of the CP energies versus phosphorous composition x in GaAs_{1-x}P_x/GaAs alloys.

In the literature, there are different values for bowing parameter of GaAsP alloys. The obtained value b in this study is in agreement with the obtained theoretically [24] for x= 0.125 [23]. On the other hand our value is smaller than twice that of the value obtained from the ellipsometric study [13]. However, our value is very close to the reported experimental values (0.174, 0.20 and 0.21 eV) [25-27].

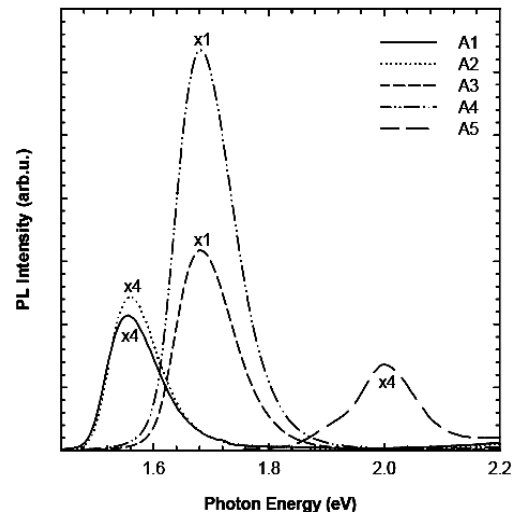


Fig. 7. PL spectra of the GaAs_{1-x}P_x/GaAs structure at room temperature.

The broadening parameters Γ versus phosphorous composition in GaAs_{1-x}P_x ternary alloys have been obtained from best fit results and they are represented in Fig. 6. As seen in this figure, the broadenings of the CP energies have increased as phosphorous composition increases. Such a behavior of Γ were also observed in the ternary alloys with antimony or nitrogen [14, 28]. The increase in broadening can be explained by the alloy scattering, statistical fluctuations, large-scale compositional variations [29].

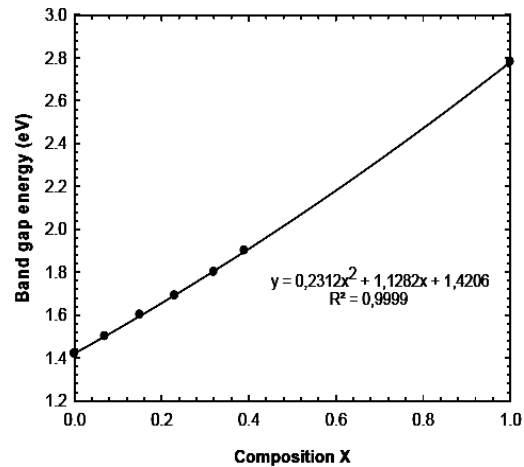


Fig. 8. Band gap energies in GaAs_{1-x}P_x/GaAs structure versus phosphorous composition x.

The increasing of the broadening of the E_0 peak is smaller than the others. The variation of alloy composition has minimal effect on the broadening of E_0 transition peak. However, E_1 and $E_1+\Delta_1$ critical points are more affected by the phosphorous induced disorder, compared to E_0 critical point. Due to this effect, the Γ_1 and $\Gamma_1+\Delta_1$ broadening parameters for GaAs_{1-x}P_x samples are increased with higher phosphorous composition. The similar behavior was also observed for GaAsSb and GaAsN in Ref 28 and 14, respectively.

It is well known that the band gap energy and alloy composition can be also estimated from peak positions of luminescence emission of the semiconductor alloys. The obtained photoluminescence spectra versus photon energy of A1-A5 samples are given in Fig. 7. It can be seen that an increase in the phosphorous composition leads to a change of the main peak position which is corresponded to band to band transitions of the samples revealed a blue-shifting. For a comparison, the band to band transition energies (band gap energies) of the alloys that the determined from SE and PL measurements are listed in the second and third column of Table 3 with respect to phosphorous composition.

Table 3. The band to band transition energies of the alloys from SE and PL measurements and phosphorous composition in the GaAsP ternary alloy from HRXRD measurements.

Sample	E_0 (eV)		Composition x (%)
	SE	PL	
A1	1.51	1.50	7.0
A2	1.62	1.60	15.0
A3	1.71	1.69	23.0
A4	1.78	1.80	32.0
A5	1.91	1.90	39.0

As seen from the table, the determined energies from these two experiments are very close each other. Also, the obtained band gap energies from the PL emission peak positions for the studied samples are plotted versus compositions x in Fig. 8. Due to a disorder of phosphorous in the structures, the band gap energies have blue-shifted with a positive bowing as the observed bowing of E_0 that the determined DF from ellipsometric data which is given in the Fig.5. The bowing parameter has been found as 0.2312 eV from the polynomial fitting seen in Fig.8. The values of the bowing obtained from both ellipsometric data and PL measurements are in good agreement in each other. Finally, it is seen that the bowing values, obtained from both PL and SE studies, clearly satisfy the Vegard law, $E_g = E_g(\text{GaAs}) + [E_g(\text{GaP}) - E_g(\text{GaAs})]x + bx^2$, with the values of $E_g(\text{GaP}) = 2.78$ eV and $E_g(\text{GaAs}) = 1.42$ eV for PL (1.43 eV for SE).

4. Conclusions

We have presented the phosphorous effect on the E_0 , E_1 , $E_1+\Delta_1$, E'_0 , and E_2 edges (CPs) of the GaAs_{1-x}P_x ternary alloys grown by MBE with different growth conditions. CP energies of the five GaAs_{1-x}P_x samples (x = 7%, 15%, 23%, 32% and 39%) have been analyzed by fitting standard critical-point line shapes to the second derivatives of the dielectric function obtained from SE measurements in the energy region of 0.5 – 5 eV. It is observed that the CPs energies of the alloys have shifted linearly to higher energies (blue-shifted) and the spin-orbit splitting (Δ_1) energy decreases by increasing phosphorous composition. The broadenings of the CP energies have increased as phosphorous composition increases due to alloy scattering, statistical fluctuations, large-scale compositional variations. However, the E_0 edge of the structures has shifted to high energies (blue-shifted) with a positive bowing as P composition increases. We have also determined a new positive bowing parameter for band gap energies of the GaAsP ternary alloys as 0.23 eV from both SE and PL measurement.

Acknowledgments

This work was supported by DPT under project No. 2001K120590.

References

- [1] J. L. Jewell, J. P. Harbison, A. Scherer, Y. H. Lee, L. T. Florez, IEEE J. Quantum Electron. **27**, 1332 (1991).
- [2] E. G. Insel, Siemens Components, Inc., Optoelectronics Div., private communications.
- [3] H. C. Kuo, Y. H. Chang, Y. A. Chang, F. I. Lai, J. T. Chu, M. N. Tsai, S. C. Wang, IEEE J. Sel. Top. Quantum Electron. **11**, 121 (2005).
- [4] S. C. Warnick, M. A. Dahleh, Proceedings of the 36th Conference on Decision & Control San Diego, California USA December, 1997.
- [5] V. A. Mishurnyi, F. de Anda, V. A. Elyukhin, I. C. Hernandez, Critical Reviews in Solid State and Materials Sciences **31**, 1 (2006).
- [6] Contributed to International Workshop on Polarized Electron Sources and Polarimeters (PESP 2004), 7-9 October 2004, Mainz, Germany.
- [7] T. Nishitani, T. Nakanishi, M. Yamamoto, S. Okumi, F. Furuta, M. Miyamoto, M. Kuwahara, N. Yamamoto, K. Naniwa, J. Appl. Phys. **97**, 094907B (2005).
- [8] A. S. Brown, M. Losurdo, P. Capezzuto, G. Bruno, T. Brown, G. May, J. Appl. Phys. **99**, 093510 (2006).
- [9] W. Shu-Dong, G. Li-Wei, W. Wen-Xin, L. Zhi-Hua, N. Ping-Juan, H. Qi, and Z. Jun-Ming, Chin. Phys. Lett. **22**(4), 960 (2005).

- [10] A. Bengi, Ş. Altındal, S. Özçelik, T. S. Mammadov, *Physica B* **396**, 22 (2007).
- [11] Y. Tatsuoka, H. Kamimoto, T. Kitada, S. Shimomura, S. Hiyamizu, *J. Vac. Sci. Technol. B* **18**(3), 1549 (2000).
- [12] A. S. Brown, M. Losurdo, P. Capezzuto, G. Bruno, T. Brown, G. May, *J. Appl. Phys.* **99**, 093510 (2006).
- [13] K. J. Kim, M. H. Lee, J. H. Bahng, K. Shim, B. D. Choe, *J. Appl. Phys.* **84**(7), 3696 (1998).
- [14] N. B. Sedrine, J. Rihani, J. L. Stehle, J. C. Harmand, R. Chtourou, *Materials Science and Engineering C* **28**, 640 (2008).
- [15] T. H. Ghong, T. J. Kim, Y. W. Jung, Y. D. Kim, D. E. Aspnes, *J. Appl. Phys.* **103**, 073502 (2008).
- [16] G. Kowalski, J. Gronkowski, A. Czyzak, T. Slupinski, J. Borowski, *Phys. Stat. Sol. A* **204**(8), 2578 (2007).
- [17] H. Fujiwara, *Spectroscopic Ellipsometry Principles and Applications*, John Wiley&Sons, 2007.
- [18] M. Erman, J. B. Theeten, P. Chambon, S. M. Kelso, D. E. Aspnes, *J. Appl. Phys.* **56**, 2664 (1984).
- [19] S. Adachi, *Phys. Rev. B* **35**, 7554 (1987).
- [20] S. Adachi, *Phys. Rev. B* **38**, 12345 (1988).
- [21] A.R. Forouhi and I. Bloomer, *Phys. Rev.* **115**, 786 (1986).
- [22] P. Lautenschlager, M. Garriga, S. Logothetidis, M. Cardona, *Phys. Rev. B* **35**, 17 (1987).
- [23] S.-H. Wei, A. Zunger, *Phys. Lett.* **76**, 664 (1996).
- [24] M. Bugajski, A. M. Kontkiewicz, H. Mariette, *Phys. Rev. B* **28**, 7105 (1983).
- [25] S. S. Vishnubhatla, B. Eyclunent, J. C. Woolley, *Can. J. Phys.* **47**, 1661 (1969), and references therein.
- [26] R. Hill, *J. Phys. C* **7**, 521 (1974).
- [27] D.E. Aspnes, *Phys. Rev. B* **14**, 5331 (1976).
- [28] N. B. Sedrine, T. Gharbi, J. C. Harmand, R. Chtourou, *Phys. Stat. Sol. A* **205**(4), 833 (2008).
- [29] C. S. Cook, S. Zollner, M. R. Bauer, P. Aella, J. Kouvetakis, J. Menendez, *Thin Solid Films* **455**, 217 (2004).

*Corresponding author: cetins@gazi.edu.tr